Downloaded from orbit.dtu.dk on: May 05, 2023

DTU Library

Fiber pull-out test and single fiber fragmentation test - analysis and modelling

Sørensen, Bent F.; Lilholt, Hans

Published in:
IOP Conference Series: Materials Science and Engineering

Link to article, DOI:
10.1088/1757-899X/139/1/012009

Publication date:
2016

Document Version
Peer reviewed version

Link back to DTU Orbit

Citation (APA):
Sørensen, B. F., & Lilholt, H. (2016). Fiber pull-out test and single fiber fragmentation test - analysis and modelling. *IOP Conference Series: Materials Science and Engineering*, *139*. https://doi.org/10.1088/1757-899X/139/1/012009

General rights
Copyright and moral rights for the publications made accessible in the public portal are retained by the authors and/or other copyright owners and it is a condition of accessing publications that users recognise and abide by the legal requirements associated with these rights.

- Users may download and print one copy of any publication from the public portal for the purpose of private study or research.
- You may not further distribute the material or use it for any profit-making activity or commercial gain
- You may freely distribute the URL identifying the publication in the public portal

If you believe that this document breaches copyright please contact us providing details, and we will remove access to the work immediately and investigate your claim.

Fiber pull-out test and single fiber fragmentation test - analysis and modelling

B F Sørensen[1] **and H Lilholt**

Section of Composites and Materials Mechanics, Department of Wind Energy, The Technical University of Denmark, Risø Campus, Frederiksborgvej 399, DK-4000 Roskilde, Denmark

[1]e-mail: bsqr@dtu.dk

Abstract. A mathematical model is developed for the analysis of the fiber debonding phase of a pull-out experiment where the matrix is supported at the same end as the fiber is loaded in tension. The mechanical properties of the fiber/matrix are described in terms of two parameters, a fracture energy for fiber/matrix debonding and a frictional sliding shear stress. Results for the debond length and fiber debond displacement are compared with results from similar models for single fiber pull-out experiments where the specimen is gripped at the end opposite to the end where the fiber is pulling-out and with results for a single fiber fragmentation test.

1. Introduction

The fiber/matrix interface plays an important role in controlling the macroscopic mechanical properties of fiber composites [1]. A number of tests involving specimens with a single fiber have been developed, such as single fiber pull-out tests, single fiber fragmentation tests and fiber push-out tests [2-4]. Yet it still remains a challenge to characterize the mechanical properties of the fiber/matrix interface for several reasons. First, the practical side. The manufacture of specimens with a single fiber involves handling of individual thin fibers which can be difficult and the testing usually requires special testing devices and measurement equipment. Second, a part of the challenge is from the theoretical side. There is a lack of agreement in which parameters to use for the characterization of the mechanical behavior of the fiber/matrix interface and there is a need for suitable theoretical models and approaches for the extraction of interface parameters from experimental data.

Historically, the mechanical properties of fiber/matrix interfaces in composites were first described in terms of a maximum interfacial shear stress [5], representing yielding of a ductile interface or interface strength in case of a brittle interface. This idea led to the development of the single-fiber fragmentation test (SFFT) in which the saturated distribution of spacings between positions of multiple fiber breaks is used to for the calculation of an interfacial shear strength [5]. More recently, it has been proposed to characterize the fiber/matrix interface in terms of a debond energy and a frictional shear stress or Coulomb friction [6-9]. Such models are motivated by observations made during SFFT testing, indicating that fiber/matrix debonding takes place progressively during monotonic loading [2]. Another test type for fiber/matrix interface characterization is fiber pull-out tests. There are (at least) two ways of performing single fiber pull-out tests. One is to clamp the specimen end opposite to the one where the fiber is loaded in tension - we will denoted this test for fiber pull-out Type 1 (PO1). Another configuration is where the specimen is supported in the matrix

material in the same end as the fiber is loaded - pull-out Type 2 (PO2). In both cases, we denote the (un-deformed) length of the free fiber by L_f and the embedded length by L.

A number of micromechanical models exist for the analysis of pull-out and SFFT tests. Several of these models are quite advanced and incorporate e.g. Poisson's effects of fiber and matrix as well as residual stresses [8-12]. Unfortunately, due to mathematical complexity many of these models require a numerical implementation to be used. It is not always easy to see how model parameters are to be extracted from experiments.

In this paper, we develop a relative simple analytical shear-lag model for the analysis of fiber pull-out Type 2 (PO2). The complete pull-out experiment, from the start to the final separation of fiber and matrix, consists of three stages: the initial *debonding and sliding* phase, the *load drop* at maximum fiber stress and the *sliding and pull-out* phase to complete pulling-out of the fiber. The model describes the fiber/matrix interface in terms of two parameters, a fiber/matrix debond energy, $\mathcal{G}_c^i$, and a constant interfacial frictional a sliding shear stress, τ_s. The model incorporates residual stresses, but neglects Poisson´s effects. This allows us to make a relative simple 1-dimensional model. We describe an approach on how the interfacial parameters are determined from the debonding/sliding phase of PO2 pull-out experiments. Unlike most previous approaches, we utilize the fact that polymer matrix composites are optical transparent so that the debond length can be measured experimentally e.g. using optical miscopy during the experiment and used as an input parameter to extract model parameters from the model.

We also compare the mathematical structure of the model with other similar models for pull-out experiments where the other end is held fixed (clamped) and with the SFFT. These test methods are closely related, see Figure 1 for a comparison.

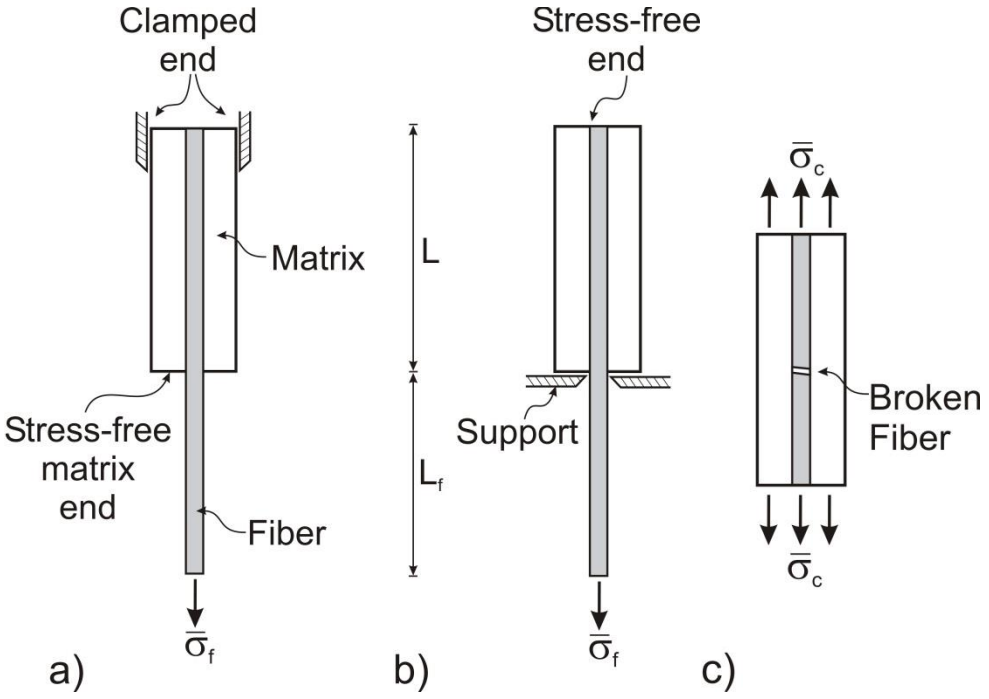

Figure 1. Comparison of testing methods (a) Pull-out Type 1 (PO1), (b) pull-out Type 2 (PO2), and (c) the single fiber fragmentation tests (SFFT).

The paper is organized as follows. First, Section 2 describes the assumption and development of the mathematical model. Next, in Section 3, we discuss the key results and explain how the interfacial parameters can be determined from experiments. Section 4 discusses the basic assumptions and limitations of the model, compares the mathematical structure of the model results with other, similar models for pull-out experiments PO1 and models for the SFFT, which are closely related, see Figure 1 for a comparison. Section 5 summarizes the major conclusions of this work.

2. Theory - model development

The section describes the basic assumption of the model, defines the geometry and boundary conditions of the model, and then the major steps in the model derivation are described.

2.1. Basic assumptions for debonding and sliding during pull-out Type 2 (PO2)

The problem we analyze is a single circular fiber embedded in a matrix cylinder. The fiber radius is r and the outer radius of the matrix cylinder is R and the fiber volume fraction is denoted V_f. The fiber has debonded a length, ℓ_d. A z-coordinate system with origin at the debonded end of the specimen is used, see Figure 2. The interfacial fracture energy is denoted $\mathcal{G}_c^i$ and the frictional sliding shear stress is τ_s. The fiber is loaded by a tensile stress, $\overline{\sigma}_f$, applied at the debonded fiber end ($z = 0$). The specimen is supported at the matrix at $z = 0$, inducing a traction $\overline{\sigma}_m$ that is in force balance with $\overline{\sigma}_f$ (note the we have defined the traction $\overline{\sigma}_m$ positive in the direction of the z-axis, opposite to the positive direction of the applied fiber stress $\overline{\sigma}_f$). As a result of the interfacial debonding and sliding, the fiber and matrix have a relative displacement δ at $z = 0$; δ is defined positive when the fiber slips out. The geometry and boundary conditions are shown in Figure 2. The fiber and matrix are taken to possess linear-elastic behavior described in terms of a Young's modulus of the fiber and matrix, denoted E_f and E_m respectively.

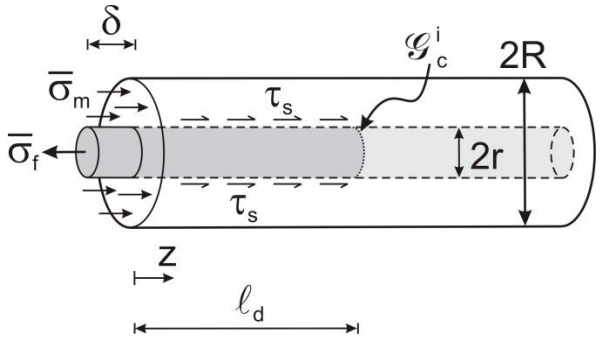

Figure 2. Geometry and loading of the model for pull-out Type 2 (PO2).

2.2. Residual stresses

The composite is taken to be stress-free at the processing temperature, T_0. However, residual stresses can be present in the unloaded composite when cooled down to the temperature, T, where the pull-out test is performed. In the following, we will express the residual stresses in terms of a mismatch strain, $\Delta\varepsilon^T$. The mismatch strain is the strain difference that would exist between fiber and matrix at the testing temperature if the fiber and matrix were allowed to expand and contract freely following the processing history. Thus, $\Delta\varepsilon^T$ can be a result of shrinkage due to cross linking of polymers chains

during curing, contraction due to thermal expansion mismatch during cool-down, etc. In the following, we will calculate the mismatch strain in case it originates solely from a mismatch in thermal expansion coefficients. With α_f and α_m being the thermal expansion coefficients of fiber and matrix, the residual stresses in the fiber and matrix induced by thermal expansion mismatch are found as (see Appendix A)

$$\frac{\sigma_f^{res}}{E_f} = -\Delta\varepsilon^T (1-V_f)\frac{E_m}{E_c} \qquad \frac{\sigma_m^{res}}{E_m} = \Delta\varepsilon^T V_f \frac{E_f}{E_c}, \tag{1}$$

where the mismatch strain is defined as

$$\Delta\varepsilon^T = \left(\alpha_f - \alpha_m\right)\left(T - T_0\right), \tag{2}$$

and E_c is the Young's modulus of the composite, given by

$$E_c = (1-V_f)E_m + V_f E_f . \tag{3}$$

In principle, residual stresses can originate from other phenomena than a mismatch in the thermal expansion coefficients. However, irrespective of their cause, residual stresses can be represented in terms of a mismatch strain, $\Delta\varepsilon^T$. Therefore the model is formulated such that $\Delta\varepsilon^T$ is considered being an unknown quantity that must be determined experimentally. Appendix A describes how to account for a pre-stress applied to the fiber during specimen manufacturing. In the present paper, we will treat three microscale parameters as unknowns that must be determined from experiments: $\mathcal{G}_c^i$, τ_s and $\Delta\varepsilon^T$.

2.3. Stresses and strains in the debonded zone

With the applied stresses at $z = 0$ being $\overline{\sigma}_f$, force balance of the specimen gives

$$\overline{\sigma}_m = \overline{\sigma}_f \frac{V_f}{(1-V_f)} . \tag{4}$$

The stresses in the debonded zone are found by force balance, accounting for the stress transfer from the fiber to the matrix via the interfacial shear stress, τ_s, which acts in the direction opposite to the slip direction at the fiber/matrix interface. The stress in the fiber at position z is:

$$\sigma_f^-(z) = \overline{\sigma}_f - 2\tau_s \frac{z}{r} \qquad \text{for } 0 \le z \le \ell_d , \tag{5}$$

(superscript "-" indicates the stress in the wake of the crack tip) and the stress in the matrix cylinder at position z is

$$\sigma_m^-(z) = \frac{V_f}{(1-V_f)}\left(2\tau_s \frac{z}{r} - \overline{\sigma}_f\right) \quad \text{for } 0 \le z \le \ell_d . \tag{6}$$

The strain in the fiber at position z within the debonded zone is obtained from Hooke's law:

$$\varepsilon_f^-(z) = \frac{\overline{\sigma}_f}{E_f} - 2\frac{\tau_s}{E_f}\frac{z}{r} + \alpha_f \Delta T \quad \text{for } 0 \le z \le \ell_d . \tag{7}$$

Likewise, we find the strain in the matrix as:

$$\varepsilon_m^-(z) = \frac{V_f}{(1-V_f)}\left\{2\frac{\tau_s}{E_m}\frac{z}{r} - \frac{\overline{\sigma}_f}{E_m}\right\} + \alpha_m \Delta T \quad \text{for } 0 \le z \le \ell_d . \tag{8}$$

2.4. Stresses far ahead of the crack tip

Far ahead of the debond crack tip (superscript "+" indicates position ahead of the debond crack tip), the stresses are independent of z -position and equal to the residual stresses:

$$\sigma_f^+(z) = \sigma_f^{res} = -\Delta\varepsilon^T (1-V_f)\frac{E_m E_f}{E_c} \qquad \textit{and} \qquad \sigma_m^+(z) = \sigma_m^{res} = \Delta\varepsilon^T V_f \frac{E_m E_f}{E_c}. \tag{9}$$

2.5. Fiber debond displacement

The fiber debond displacement at position $z = 0$, δ, is obtained by integration of the strain difference along the sliding part of the interface, assuming that there is no displacement difference (slip) between the fiber and matrix at the crack tip ($z = \ell_d$):

$$\delta = \int_0^{\ell_d} \left[\varepsilon_f^-(z) - \varepsilon_m^-(z)\right] dz. \tag{10}$$

The debond displacement in (10) is defined to be positive when the fiber slips out of the matrix. Inserting $\varepsilon_f^-(z)$ and $\varepsilon_m^-(z)$ from (7) and (8) into (10) and performing the integration leads to:

$$\frac{\delta}{r} = \left(\frac{E_c}{(1-V_f)E_m}\frac{\overline{\sigma}_f}{E_f} + \Delta\varepsilon^T\right)\left(\frac{\ell_d}{r}\right) - \frac{E_c}{(1-V_f)E_m}\frac{\tau_s}{E_f}\left(\frac{\ell_d}{r}\right)^2. \tag{11}$$

Eq. (11) is the first major result of our analysis. Eq. (11) can be re-written as follows:

$$\Delta\varepsilon^T = \left(\frac{\delta}{\ell_d}\right) + \frac{E_c}{(1-V_f)E_m}\left[\frac{\tau_s}{E_f}\left(\frac{\ell_d}{r}\right) - \frac{\overline{\sigma}_f}{E_f}\right]. \tag{12}$$

Eq. (12) enables the determination of $\Delta\varepsilon^T$ from experimental measurements of ℓ_d and δ as a function of the applied fiber stress, $\overline{\sigma}_f$, if the interfacial shear stress τ_s is determined independently. Note that Eq. (12) is independent of $\mathcal{G}_c^i$.

2.6. Determination of debond length

In order to establish equations for the determination of $\mathcal{G}_c^i$ and τ_s, we proceed to determine the debond length ℓ_d as a function of the applied fiber stress, $\overline{\sigma}_f$. To do so, we utilize the potential energy approach of Budiansky, Hutchinson and Evans [13]. This approach is developed to calculate the potential energy loss accounting for large-scale frictional sliding. More precisely, the approach calculates the potential energy differences of two states of a cracked body with fixed surface tractions as it undergoes further cracking and frictional sliding. In State I, the body is subjected to surface tractions and cracks are present and frictional slippage has occurred along internal interfaces in the body. The body now undergoes further debonding and frictional slipping to State II. During this transition, frictional shear stresses perform further work and thus dissipates energy. Utilizing the principle of virtual work, Budiansky *et al*. [13] were able to eliminate the work of the applied tractions and express the potential energy difference between the two states as follows:

$$\Pi_I - \Pi_{II} = \frac{1}{2}\int_V (\sigma_I - \sigma_{II}) : M(\sigma_I - \sigma_{II}) dV + \xi_F, \tag{13}$$

where Π_I and Π_{II} are the potential energy of State I and State II. In (13), V is the volume of the body, σ_I and σ_{II} are the stresses associated with State I and State II, M indicates an elastic operator (Hooke's law) and ξ_F is the frictional energy dissipation, defined as

$$\xi_F = \tau_s \int_{S_F} |\Delta u| \, dS \, . \tag{14}$$

In (14), $|\Delta u|$ denotes the relative frictional slip between the two states (assumed to occur monotonically during the transition from State I to State II) and S_F is the surface area at which frictional sliding occurs.

The potential energy loss will be available for the energy absorption and dissipation during the transition from State I to State II. Therefore, a criterion for debond crack growth can be stated as follows: The debond crack propagation will occur only when the potential energy loss, eq. (13), is equal to the energy absorption by the debonding of the fiber/matrix crack tip and the frictional energy dissipation. This can be written as:

$$\Pi_I - \Pi_{II} = \mathcal{G}_c^i \, 2\pi r \, \Delta\ell_d + \xi_F \, . \tag{15}$$

The right hand side of Eq. (15) is the energy absorption by the debonding of the fiber/matrix crack tip and the frictional energy dissipation. Inserting (13) into the left hand side of (15), we note that the frictional energy dissipation term, ξ_F, will appear on both sides in (15) and thus will cancel out. This is a major advantage of the approach since it simplifies the calculations; the frictional energy dissipation and (it turns out) the potential of the applied tractions do not need to be calculated.

We first identify State I as the problem of a debond length ℓ_d and State II as the situation where the debond crack length has increased by a small distance, $\Delta\ell_d$. We note that with the tractions at the external boundaries held fixed, the State II stresses, $\sigma_f^-(z)$ and $\sigma_m^-(z)$, in the region $0 < z < \ell_d$, are exactly the same as for State I. In State II, the length of the slip zone has increased by $\Delta\ell_d$, so the equations (4) and (5) for $\sigma_f^-(z)$ and $\sigma_m^-(z)$ are now valid also for the new (State II) slip zone, $0 \le z \le \ell_d + \Delta\ell_d$. The upstream stresses, σ_f^+ and σ_m^+, are unchanged for $z > \ell_d + \Delta\ell_d$. Then, for the transition from State I to State II, the stress state changes only for $\ell_d < z < \ell_d + \Delta\ell_d$. Therefore, (13) becomes

$$\Pi_I - \Pi_{II} = \frac{1}{2} \int_{\ell_d}^{\ell_d + \Delta\ell_d} \left\{ \pi r^2 \frac{\left(\sigma_f^+ - \sigma_f^-(z)\right)^2}{E_f} + \pi\left(R^2 - r^2\right) \frac{\left(\sigma_m^+ - \sigma_m^-(z)\right)^2}{E_m} \right\} dz + \xi_F \, . \tag{16}$$

Omitting details (the analyses presented here follows that of Sørensen [14] who analyzed fiber failure and progressive debonding of a SFFT using a similar approach), we insert σ_f^+ and σ_m^+ from (9) and $\sigma_f^-(z)$ and $\sigma_m^-(z)$ from (5) and (6) into (16). After having performed the integration, we neglect higher order terms of $\Delta\ell_d$ (since $\Delta\ell_d << \ell_d$), and insert the result for the potential energy loss into the left hand side of (15). Then, $\Delta\ell_d$ appears on all terms on both sides and cancels out. We end up with an equation for the determination of the debond length, ℓ_d. For $\tau_s \neq 0$ we get

$$\frac{\ell_d}{r} = \frac{E_f}{2\tau_s} \left(\frac{\overline{\sigma}_f}{E_f} + \frac{(1 - V_f) E_m}{E_c} \Delta\varepsilon^T \right) - \frac{E_f}{\tau_s} \sqrt{\frac{(1 - V_f) E_m}{E_c} \left(\frac{\mathcal{G}_c^i}{E_f r} \right)} \, . \tag{17}$$

Eq. (17) is our second major result. From (17) we note that the debond length depends on all three unknown parameters, $\mathcal{G}_c^i$, τ_s and $\Delta\varepsilon^T$.

3. Further analysis

In this section we re-write and combine equations (11) and (17) to forms that are particularly suited for use in connection with experimental determination of the unknown parameters, $\mathcal{G}_c^i$, τ_s and $\Delta\varepsilon^T$.

3.1. Re-arranging equations

We can rewrite (17) to give $\bar{\sigma}_f$ as a function of ℓ_d:

$$\frac{\bar{\sigma}_f}{E_f} = 2\sqrt{\frac{(1-V_f)E_m}{E_c}\left(\frac{\mathcal{G}_c^i}{E_f r}\right)} - \frac{(1-V_f)E_m}{E_c}\Delta\varepsilon^T + 2\frac{\tau_s}{E_f}\left(\frac{\ell_d}{r}\right). \tag{18}$$

We define the fiber stress corresponding to debond initiation as the value of $\bar{\sigma}_f$ for $\ell_d = 0$:

$$\frac{\bar{\sigma}_f^i}{E_f} = 2\sqrt{\frac{(1-V_f)E_m}{E_c}\left(\frac{\mathcal{G}_c^i}{E_f r}\right)} - \frac{(1-V_f)E_m}{E_c}\Delta\varepsilon^T, \tag{19}$$

so that (18) can be written as

$$\frac{\bar{\sigma}_f}{E_f} = \frac{\bar{\sigma}_f^i}{E_f} + 2\frac{\tau_s}{E_f}\left(\frac{\ell_d}{r}\right). \tag{20}$$

Eq. (20) shows that $\bar{\sigma}_f$ is related linearly to ℓ_d. This suggests an experimental way to determine the interfacial frictional shear stress from the slope of the $\bar{\sigma}_f$ - ℓ_d relationship. Differentiation of (20) leads to:

$$\tau_s = \frac{r}{2}\left(\frac{d\bar{\sigma}_f}{d\ell_d}\right). \tag{21}$$

Thus, by recording the relationship between $\bar{\sigma}_f$ and ℓ_d we can determine τ_s from (21). Eq. (21) is our third major result.

We now insert ℓ_d from (17) into (11). The result is

$$\frac{\delta}{r} = \frac{1}{4}\frac{(1-V_f)E_m}{E_c}\frac{E_f}{\tau_s}\left(\frac{E_c}{(1-V_f)E_m}\frac{\bar{\sigma}_f}{E_f} + \Delta\varepsilon^T\right)^2 - \frac{\mathcal{G}_c^i}{\tau_s r}. \tag{22}$$

Rewriting (19), we obtain

$$\frac{\mathcal{G}_c^i}{E_f r} = \frac{1}{4}\frac{(1-V_f)E_m}{E_c}\left(\frac{\bar{\sigma}_f^i}{E_f} + \frac{(1-V_f)E_m}{E_c}\Delta\varepsilon^T\right)^2. \tag{23}$$

This result, which is our fourth important result, is independent of τ_s but requires the knowledge of $\Delta\varepsilon^T$. Eq. (23) thus provides one equation to determine $\mathcal{G}_c^i$ from measured values of $\bar{\sigma}_f^i$ and $\Delta\varepsilon^T$, i.e. one result per test specimen.

Inserting $\Delta\varepsilon^T$ from (12) into (23) gives

$$\frac{\mathcal{G}_c^i}{E_f r} = \frac{1}{4}\frac{E_c}{(1-V_f)E_m}\left(\frac{\bar{\sigma}_f - \bar{\sigma}_f^i}{E_f} + \frac{(1-V_f)E_m}{E_c}\left(\frac{\delta}{\ell_d}\right) + \frac{\tau_s}{E_f}\left(\frac{\ell_d}{r}\right)\right)^2. \tag{24}$$

This, our fifth main result, is independent of $\Delta\varepsilon^T$. Unlike the result (23), Eq. (24) enables the determination of multiple values of $\mathcal{G}_c^i$ from multiple sets of data ($\bar{\sigma}_f$, ℓ_d and δ) from one test

specimen. This approach is thus likely to provide a more accurate estimate of $\mathcal{G}_c^i$ that the result based on a single data set, Eq. (23).

3.2. Approximations for $V_f \to 0$

A further simplification of results can be obtained by considering $V_f \to 0$, which is practically the case for specimens consisting of a single fiber cast into a matrix specimen. First we note that $E_c \to E_m$ for $V_f \to 0$, so that $(1-V_f)E_m/E_c \to 1$ for $V_f \to 0$. Then (12) reduces to

$$\Delta\varepsilon^T = \left(\frac{\delta}{\ell_d}\right) + \left[\frac{\tau_s}{E_f}\left(\frac{\ell_d}{r}\right) - \frac{\bar{\sigma}_f}{E_f}\right], \tag{25}$$

while (19) simplifies to

$$\frac{\bar{\sigma}_f^i}{E_f} = 2\sqrt{\frac{\mathcal{G}_c^i}{E_f r}} - \Delta\varepsilon^T, \tag{26}$$

while eq. (22) becomes

$$\frac{\delta}{r} = \frac{1}{4}\frac{E_f}{\tau_s}\left(\frac{\bar{\sigma}_f}{E_f} + \Delta\varepsilon^T\right)^2 - \frac{\mathcal{G}_c^i}{\tau_s r}, \tag{27}$$

and (24) reduces to

$$\frac{\mathcal{G}_c^i}{E_f r} = \frac{1}{4}\left(\frac{\bar{\sigma}_f - \bar{\sigma}_f^i}{E_f} + \left(\frac{\delta}{\ell_d}\right) + \frac{\tau_s}{E_f}\left(\frac{\ell_d}{r}\right)\right)^2. \tag{28}$$

Finally, eq. (23) can be written as

$$\frac{\mathcal{G}_c^i}{E_f r} = \frac{1}{4}\left(\frac{\bar{\sigma}_f^i}{E_f} + \Delta\varepsilon^T\right)^2. \tag{29}$$

Eq. (29) is simply another form of (26).

3.3. Approach for parameter determination

We will now describe an approach for the determination of the interface parameters $\mathcal{G}_c^i$ and τ_s as well as the strain mismatch, $\Delta\varepsilon^T$, from measurement from a continuous pull-out Type 2 (PO2) test. The procedure follows a similar procedure proposed earlier for the pull-out Type 1 (PO1) [15]. We assume that during the single fiber pull-out experiments the parameter $\bar{\sigma}_f$, δ and ℓ_d are recorded simultaneously. We propose the following approach to determine the three parameters in three steps:

Step 1: $\bar{\sigma}_f$ is plotted as a function of ℓ_d. Since, according to (20), $\bar{\sigma}_f$ should depend linearly on ℓ_d, a straight line can be fitted to the data. This allows the determination of τ_s using (21). A sketch of such a plot is shown in Figure 3a.

Step 2: Having determined τ_s, another plot is made in accordance with (12) or (25) using the experimental values of $\bar{\sigma}_f$, δ and ℓ_d. The result should be a constant value, $\Delta\varepsilon^T$. An average value of $\Delta\varepsilon^T$ can be determined from such data. A sketch of such a plot is shown in Figure 3b.

Step 3: Knowing τ_s, the value of $\mathcal{G}_c^i$ can now be determined by the use of (24) or (29), from a plot showing $\mathcal{G}_c^i$ as a function of $\bar{\sigma}_f$ or ℓ_d using the associated values of δ. A sketch of such a plot is shown in Figure 3c.

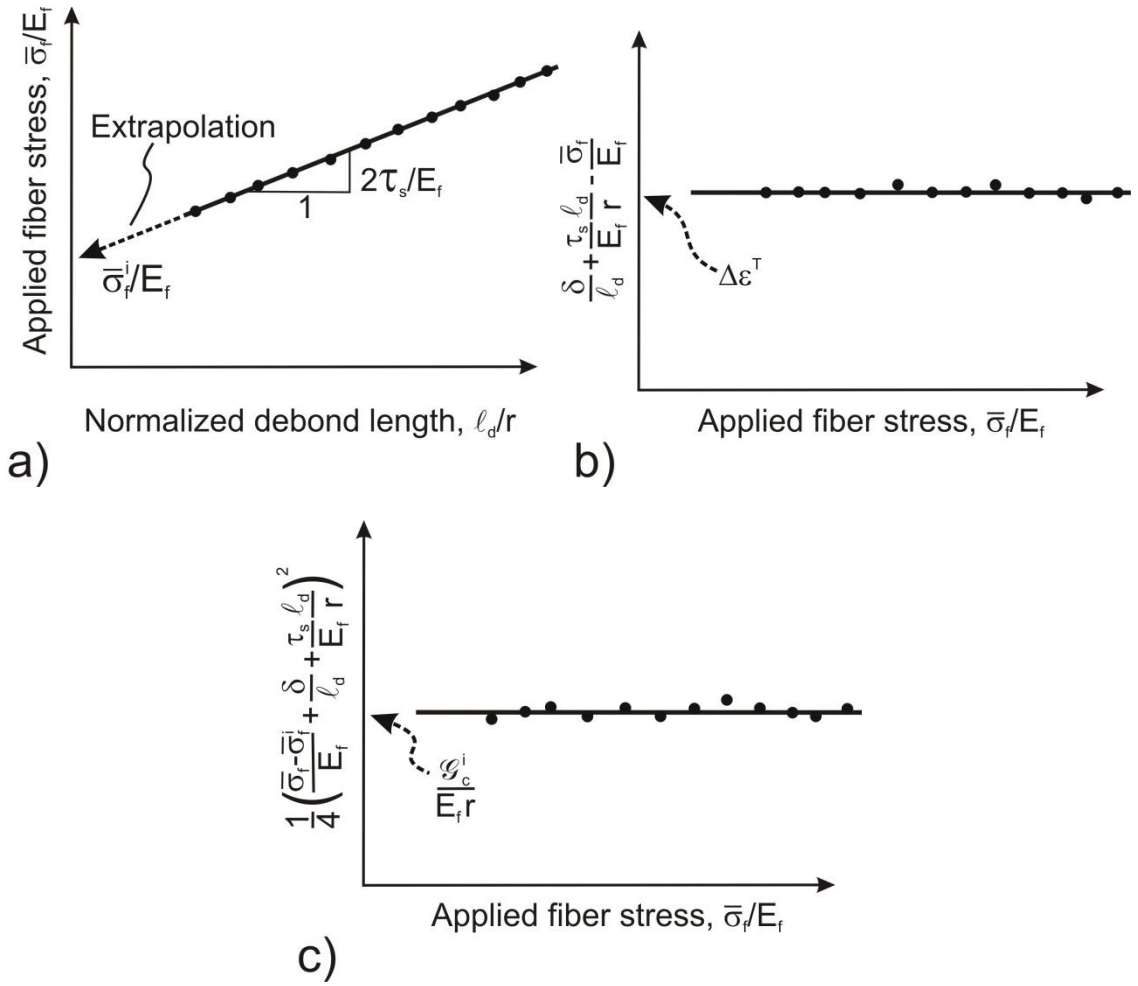

Figure 3. Sketches of plots for the determination of parameters τ_s, $\Delta\varepsilon^T$ and $\mathcal{G}_c^i$ from data from pull-out experiments. (a) A plot of $\bar{\sigma}_f$ as a function of ℓ_d for the determination of τ_s according to (21). (b) Plot of experimental values of $\bar{\sigma}_f$, δ and ℓ_d combined according to Eq. (25) to give $\Delta\varepsilon^T$. (c) Values of $\bar{\sigma}_f$, δ and ℓ_d combined according to (28) to give $\mathcal{G}_c^i$.

An independent check of $\mathcal{G}_c^i$ can be made by (23) or (28) where first $\bar{\sigma}_f^i$ is determined from a plot showing $\bar{\sigma}_f$ as a function of ℓ_d (as Figure 3a) by extrapolation to ℓ_d = 0, and then using $\bar{\sigma}_f^i$ and $\Delta\varepsilon^T$ in (23). It should be noted that $\bar{\sigma}_f^i$ cannot be obtained directly as the experimental stress value where debonding is found to initiate in the experiments, because the model is not really valid for initiation. Having determined all the parameters, $\mathcal{G}_c^i$, τ_s and $\Delta\varepsilon^T$, we can make a another check of

the accuracy of the parameters by plotting $\overline{\sigma}_f$ as a function of δ, using eq. (22), and compare the predicted graph with the original experimental data for $\overline{\sigma}_f$ as a function of δ.

4. Discussion

In the following, we will compare the equations of the present analysis for PO2 with similar equations for PO1 and SFFT. We also discuss the pull-out part of the experiment and the major assumptions of the present model.

4.1. Comparison with results from other pull-out and SFFT problems

The three basic test problems, PO1, PO2 and SFFT (Figure 2) can be considered as special cases of a more general problem, where there are three applied stresses, $\overline{\sigma}_f$ and $\overline{\sigma}_m$ applied to the fiber and matrix at $z = 0$ and a stress $\overline{\sigma}_c$ applied to the uncracked end of the composite specimen at $z = L$, see Figure 4. Care needs to be taken on the direction of sliding and pull-out and the sign (direction) of the frictional shear stress - note that the sliding direction of the SFFT is opposite to the pull-out tests. Force equilibrium gives

$$\overline{\sigma}_c - V_f \overline{\sigma}_f + (1 - V_f)\overline{\sigma}_m = 0 . \tag{30}$$

The three cases PO1, PO2 and SFFT correspond to the following conditions for the applied stresses:

$\overline{\sigma}_m = 0$ corresponds to PO1

$\overline{\sigma}_c = 0$ corresponds to PO2

$\overline{\sigma}_f = 0$ corresponds to SFFT

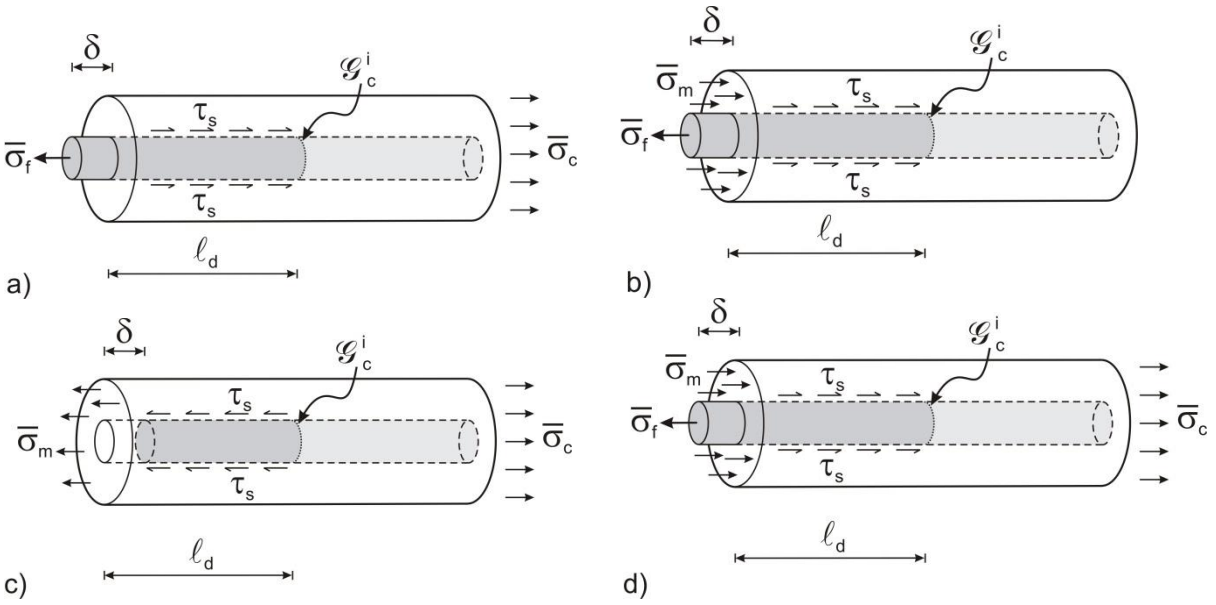

Figure 4. Models for (a) pull-out Type 1 (PO1), (b) pull-out Type 2 (PO2), (c) SFFT and (d) general model.

The conditions enter the equations for the stresses $\sigma_f^-(z)$, $\sigma_m^-(z)$, σ_f^+, σ_m^+, corresponding to (5), (6) and (9) for case PO2, and thus affects the results for the debond length ℓ_d and the relative displacement, δ. Let us compare the equation for $\overline{\sigma}_f$ versus ℓ_d for the two pull-out cases.

For PO1, the equation for $\overline{\sigma}_f$ as a function of ℓ_d is given by Hutchinson and Jensen [8]:

$$\frac{\overline{\sigma}_f^{PO1}}{E_f} = 2\frac{E_c}{(1-V_f)E_m}\sqrt{\frac{(1-V_f)E_m}{E_c}\left(\frac{\mathcal{G}_c^i}{E_f r}\right)} - \Delta\varepsilon^T + 2\frac{\tau_s}{E_f}\left(\frac{E_c}{(1-V_f)E_m}\right)\left(\frac{\ell_d}{r}\right). \tag{31}$$

Superscripts indicate test method. For PO2, the result is given by Eq. (18), reproduced below:

$$\frac{\overline{\sigma}_f^{PO2}}{E_f} = 2\sqrt{\frac{(1-V_f)E_m}{E_c}\left(\frac{\mathcal{G}_c^i}{E_f r}\right)} - \frac{(1-V_f)E_m}{E_c}\Delta\varepsilon^T + 2\frac{\tau_s}{E_f}\left(\frac{\ell_d}{r}\right). \tag{32}$$

It is seen that the result for PO2 is simply the result of PO1 multiplied by $(1-V_f)E_m/E_c$. This implies that for the same ℓ_d the stresses scales according to:

$$\sigma_f^{PO2} = \frac{(1-V_f)E_m}{E_c}\overline{\sigma}_f^{PO1}. \tag{33}$$

Next we compare the equations for δ as a function of $\overline{\sigma}_f$ for the two pull-out cases. For PO1 we have [8]:

$$\frac{\delta^{PO1}}{r} = \frac{1}{4}\frac{(1-V_f)E_m}{E_c}\frac{E_f}{\tau_s}\left(\frac{\overline{\sigma}_f^{PO1}}{E_f} + \Delta\varepsilon^T\right)^2 - \frac{\mathcal{G}_c^i}{\tau_s r}, \tag{34}$$

while for PO2 we have eq. (22):

$$\frac{\delta^{PO2}}{r} = \frac{1}{4}\frac{(1-V_f)E_m}{E_c}\frac{E_f}{\tau_s}\left(\frac{E_c}{(1-V_f)E_m}\frac{\overline{\sigma}_f^{PO2}}{E_f} + \Delta\varepsilon^T\right)^2 - \frac{\mathcal{G}_c^i}{\tau_s r}. \tag{35}$$

We see that these equations are identical if the applied stress terms in the brackets are equal, i.e. under the condition

$$\overline{\sigma}_f^{PO1} = \frac{E_c}{(1-V_f)E_m}\overline{\sigma}_f^{PO2}. \tag{36}$$

This is the same relationship as above, eq. (33). Thus, for the same ℓ_d and same δ the stresses scale by the factor $(1-V_f)E_m/E_c$. This factor is very close to, but slightly lower than unity for a single fibre composite specimen because from (3), $E_c \to E_m$ for $V_f \to 0$. This shows that there is very little difference in terms of stresses and pull-out displacement for the two pull-out cases, PO1 and PO2.

A similar comparison of equations for ℓ_d and δ for the SFFT case [14] gives the following scaling factors, noting that during a SFFT experiment it is the composite stress $\overline{\sigma}_c$ that is recorded, since in the SFFT the fiber is broken and thus stress free where debonding occurs.

$$\overline{\sigma}_c^{SFFT} = -\frac{(1-V_f)E_m}{E_f}\overline{\sigma}_f^{PO1}. \tag{37}$$

Again, if we consider $V_f \to 0$ we obtain

$$\bar{\sigma}_c^{SFFT} = -\frac{E_m}{E_f}\bar{\sigma}_f^{PO1}, \tag{38}$$

so that, with all parameters (including ℓ_d and δ) held fixed, the stresses are scaled approximately as the ratio of the stiffnesses of the matrix and fiber. This can be a significant difference for a polymer matrix composite where the Young's modulus of the matrix is usually significantly lower than that of the fiber. The comparison reveals that the applied composite stress of the SFFT - for the same ℓ_d - is much lower than the fiber stress of the PO1 experiment. It might be of interest to design experiments to test this relationship.

4.2. Comments regarding the full pull-out experiment

PO2 pull-out experiments are usually conducted in "displacement control", i.e. the position of the free end of the fiber is displaced in the negative z-direction at a constant rate. Such experiments can be considered to take place in two phases. In the first debonding and sliding phase, the applied load to the fiber increases and the debond crack tip propagates along the fiber towards the un-cracked end of the specimen ($z = L$) and the applied fiber stress increased. In the sliding/pull-out phase, the fiber is fully debonded and slides along the entire fiber/matrix interface, and the stress carried by the fiber is given by the frictional shear stress and the embedded fiber length, ℓ_s. The following considerations are valid for experiments being conducted in "displacement control", i.e. when the position of the free end of the fiber is displaced in the negative z-direction at a constant rate.

For the first debonding/sliding phase, our equations for the stress-displacement (22) is expected to be valid until the crack tip stress field approaches the end of the specimen, i.e. until $\ell_d \approx L$. The maximum applied fiber stress $\bar{\sigma}_f^c$ can thus be estimated from by setting $\ell_d = L$ in (20). The result is

$$\frac{\bar{\sigma}_f^c}{E_f} = \frac{\bar{\sigma}_f^i}{E_f} + 2\frac{\tau_s}{E_f}\left(\frac{L}{r}\right), \tag{39}$$

and the corresponding debond displacement is found by inserting $\bar{\sigma}_f^c$ from (39) into (11), giving

$$\frac{\delta^c}{r} = \frac{E_c}{(1-V_f)E_m}\left[\frac{\bar{\sigma}_f^i}{E_f}\left(\frac{L}{r}\right) + \frac{\tau_s}{E_f}\left(\frac{L}{r}\right)^2\right] + \Delta\varepsilon^T\left(\frac{L}{r}\right). \tag{40}$$

Just as the debond crack tip reaches the end of the specimen, the crack tip stress field vanishes and during the remainder of the experiment, the stress field is independent of $\mathcal{G}_c^i$ and $\Delta\varepsilon^T$. The stress field is now controlled by the interfacial friction and the experiments starts its sliding/pull-out phase. As this happens, the applied fiber stress drops to a value denoted $\bar{\sigma}_f^d$. The value of $\bar{\sigma}_f^d$ depends on τ_s and the initial free fiber length, L_f (see definition of L_f in Figure 1a).

In the sliding phase, the stress carried by the fiber is controlled by the frictional shear stress and the embedded fiber length, ℓ_s, along which the interfacial sliding shear stress τ_s acts. A simple force balance gives:

$$\bar{\sigma}_f = 2\tau_s\frac{\ell_s}{r}. \tag{41}$$

Clearly, the embedded fiber length ℓ_s decreases with increasing pull-out. However, the exact value of ℓ_s depends on the initial length of the free part of the fiber, i.e. the initial distance from the gripping point of the fiber to the start of the specimen, L_f. This is because the applied load level $\bar{\sigma}_f$

decreases during the sliding phase of the pull-out experiment as the embedded sliding length ℓ_s decreases (see (41). Then, the matrix-free part of the fiber unloads too and thus contracts elastically. Being griped at the loaded fiber end ($z = -L_f$), the fiber pulls out of the matrix and thus decreases the embedded length, ℓ_s. The longer the initial free length, the larger will the elastic contraction and thus the larger shortening of ℓ_s and thus the lower will $\overline{\sigma}_f^d$ be. The smallest possible load drop will be to consider $L_f = 0$, corresponding to that the fiber is gripped at $z = 0$. Then, the sliding length just after complete debonding $\ell_s^d \approx L$. An upper bound for $\overline{\sigma}_f^d$ is thus

$$\overline{\sigma}_f^d = 2\tau_s \frac{L}{r}. \tag{42}$$

From (39) and (42) it follows that this stress drop is $\overline{\sigma}_f^i$. The fiber stress $\overline{\sigma}_f$ will decrease linearly with ℓ_s in accordance with (41) and $\overline{\sigma}_f$ will vanish for $\delta = L$ corresponding to $\ell_s = 0$. Figure 5 shows a sketch of the entire $\overline{\sigma}_f - \delta$ relationship.

Relation (41) has been widely used to characterize the interfacial shear stress of pull-out experiments. It is clear from our model perspective that the use of relations like (41) is only relevant for characterization of the frictional sliding resistance of the fiber/matrix interface. It will not be useful to characterize the chemical bonding between fiber and matrix, because the bond rupture occurs in the first phase (debonding/sliding) of the experiment where the applied fiber stress is rising.

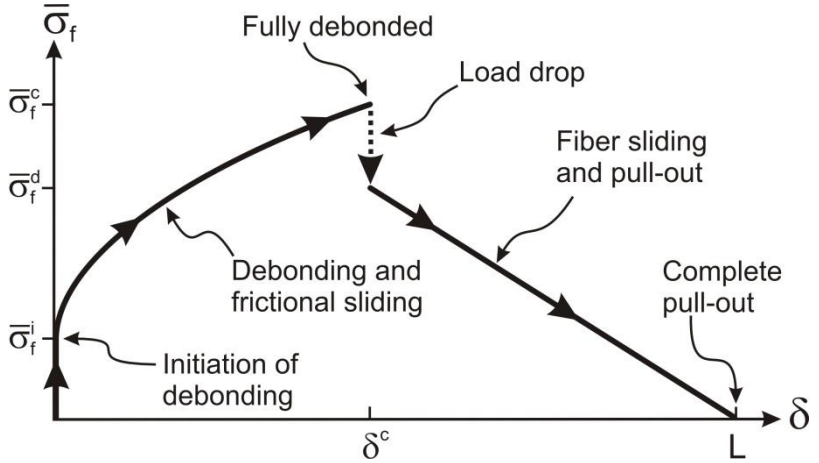

Figure 5. Sketch (not made to scale) of the fiber stress and debonding/sliding and sliding/pull-out displacement behavior of a pull-out type 2 (PO2) experiment.

4.3. Traditional analysis of pull-out experiments

An "apparent" average shear stress, calculated from the maximum applied force, $P_{\max}$, has sometimes been used to characterize the fiber/matrix interface. In connection with our analysis we obtain

$$\tilde{\tau}_s = \frac{P_{\max}}{2\pi r L} = \frac{\overline{\sigma}_f^c r}{2L} = \frac{\overline{\sigma}_f^i}{2}\frac{r}{L} + \tau_s. \tag{43}$$

It is clear that such an approach does not enable a clear separation of the interface parameters, $\mathcal{G}_c^i$ and τ_s, since $\overline{\sigma}_f^c$ depends on both parameters ($\mathcal{G}_c^i$ through $\overline{\sigma}_f^i$), see (39). Moreover, in case of non-zero $\overline{\sigma}_f^i$, the use of (43) will result in different values for $\tilde{\tau}_s$ for different values of L. This is

because $\bar{\sigma}_f^c$ is linear but not directly proportional to L, see (39); the term $\bar{\sigma}_f^i$ depends on both $\mathcal{G}_c^i$ and $\Delta\varepsilon^T$, see (19). This can be seen by considering Figure 6, which shows the theoretical relationship between $\bar{\sigma}_f$ and ℓ_d, eq (20). Consider three specimens having different initial fiber embedded length, L_1, L_2 and L_3. The associated maximum fiber stresses of the three specimens, $\bar{\sigma}_f^{c,1}$, $\bar{\sigma}_f^{c,2}$ and $\bar{\sigma}_f^{c,3}$ are indicated. The different slopes of the dashed lines indicate that the apparent shear stress $\tilde{\tau}_s$ calculated using (43) would come out differently for different values of L.

The constant term in (39), $\bar{\sigma}_f^i$, can be positive or negative depending on the values of $\mathcal{G}_c^i$ and $\Delta\varepsilon^T$. If $\bar{\sigma}_f^i$ is positive (as shown in Figure 6), the apparent shear stress $\tilde{\tau}_s$ will decrease with increasing embedded fiber length and, conversely, if $\bar{\sigma}_f^i$ is negative (in case the fiber is pre-debonded), $\tilde{\tau}_s$ will increase with increasing embedded length.

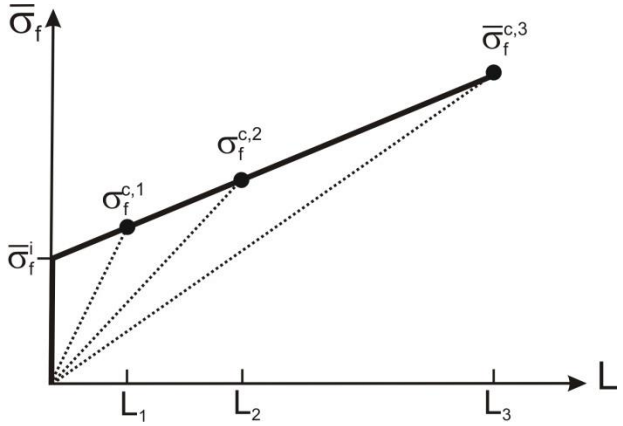

Figure 6. Sketch of the stress-debond length relationship, eq. (39), of a pull-out Type 2 (PO2) experiments with specimens of different lengths. Slopes of dashed lines indicate the apparent shear stress $\tilde{\tau}_s$.

Eq. (43) suggest a consistent way to analyze old data from traditional pull-out experiments and obtain τ_s from measurements of $\tilde{\tau}_s$ as a function of L. We note from (43) that $\tilde{\tau}_s \to \tau_s$ for $L \to \infty$ or $r/L \to 0$. Thus, if $\tilde{\tau}_s$ is plotted as a function of r/L, we can read off the true frictional shear stress τ_s at $r/L = 0$. The slope of the plot will be $\sigma_f^i/2$. According to (19), the parameter $\bar{\sigma}_f^i$ depends on both $\mathcal{G}_c^i$ and $\Delta\varepsilon^T$. Having determined $\bar{\sigma}_f^i$ from the slope of the plot, we cannot determine $\mathcal{G}_c^i$ and $\Delta\varepsilon^T$ independently but only in the combination given by (19).

4.4. Model approximations

The present model builds on a number of assumptions, such as taking fiber and matrix as linearly-elastic materials and neglecting Poisson's ratio's effects, effectively creating a one-dimensional model. Most fibers used in engineering composites, such as glass fibers and carbon fibers possess rather small non-linearity in their stress-strain behavior. The neglecting of Poisson's effects requires a few comments. First, for some fibers such as carbon fibers the Poisson's ratio is not readily known. Secondly, the Poisson's effects would induce a lateral contraction in fibers in pull-out experiments, possibly changing (reducing) the interfacial normal stress acting normal to the fiber/matrix interface. Considering Coulomb friction, a decrease in the normal stress across the interface could change

(decrease) the frictional shear stress. However, there are also experiments that indicate that roughness asperities of the fiber surface affects the frictional sliding behavior of fibers in a composite material [3, 16]. With these complexities in mind, a friction law based on a constant frictional shear stress can be seen as a crude approximation. We think, however, that the most important point is that we characterize the fiber/matrix interface in terms of two parameters that represent two distinctive physical phenomena, the debond process, in which breakage of chemical bonds are the main feature, and frictional sliding resistance. Each of the two phenomena can be modelled in various ways, but how this should be done should be based on careful physical observations.

The assumption that the mechanical behavior of the fiber/matrix interface can be adequately be described in terms of $\mathcal{G}_c^i$ and τ_s can to some extend be checked with the proposed approach outlined in Section 3.2 in which parameters are determined from combinations of measured experimental data ($\bar{\sigma}_f$ as a function of ℓ_d) which according to (20) should result in linear relationships, as outlined in Figure 3a. In case the plots show that the experimental data come out with non-linear relationships, we must conclude that the models do not represent the experiments well. Then, more advanced interface model concepts should be explored.

Finally a remark about the use of shear-lag model for the present problem. This is expected to be a fairly good approximation when the debond crack length is long. Hutchinson and Jensen [8] showed by comparing results from a shear-lag model with results from a more accurate numerical model that shear-lag models can be good approximations once the debond length is longer than about 2 -3 times *r*. This implies that the model is best suited for composites with relatively low values for the interface shear stress and debond energy.

5. Concluding remarks

An analytical model was developed for debonding and sliding of a single fiber specimen supported at the matrix at the end where the fiber is loaded in tension. The model takes the fracture energy for fiber/matrix debonding, the interfacial sliding fraction and a strain mismatch as unknowns that must be determined from experimental measurements. An approach is presented for sequential identification of these parameters. Equations for debond length and fiber debond displacement were found to have similar form as equations derived for single fiber pull-out testing where the specimen is gripped at the opposite end and for single fiber fragmentation tests.

Acknowledgements

This study was funded by the "Danish Centre for Composite Structure and Materials for Wind Turbines (DCCSM)", fund no. 09-067212 from the Danish Council for Strategic Research.

Nomenclature

ℓ_d	debond length
ℓ_s	embedded (sliding) length during pull-out phase
r	fibre radius
z	coordinate axis
E_c	Young's modulus of the composite
E_f	Young's modulus of the fibre
E_m	Young's modulus of the matrix material

$\mathcal{G}_c^i$	interfacial fracture energy
L	length of embedded part of the fibre (debond and sliding phase)
L_f	length of free fibre
R	radius of matrix cylinder
S_F	surface area where frictional slip occurs
T	temperature at which pull-out experiment is conducted
T_0	temperature at specimen is free of residual stresses
V	volume of test specimen
V_f	fibre volume fraction
α_f	thermal expansion coefficient of fibre
α_m	thermal expansion coefficient of matrix
δ	relative displacement between fibre and matrix at $z = 0$
δ^c	relative displacement between fibre and matrix at end of debonding phase ($\ell_d = L$)
$\Delta\varepsilon^T$	mismatch strain
Δu	relative slip between fibre and matrix along the fibre matrix interface
ε_f^-	strain in the fibre in the debonded/slipping zone ($z < \ell_d$)
ε_m^-	strain in the matrix in the debonded/slipping zone ($z < \ell_d$)
σ_I	stresses associated with State I
σ_{II}	stresses associated with State II
$\overline{\sigma}_c$	applied composite stress at the un-cracked end ($z = L$)
$\overline{\sigma}_f$	applied stresses at the fibre end ($z = 0$)
$\overline{\sigma}_f^c$	applied fibre stress at end of debonding phase ($\ell_d = L$)
$\overline{\sigma}_f^d$	applied fibre stress at end of beginning of the pull-out phase
$\overline{\sigma}_f^i$	applied fibre stress at initiation of fibre/matrix debonding and sliding
σ_f^-	stress in the fibre in the debonded/slipping zone ($z < \ell_d$)
σ_f^+	stress in the fibre ahead of the debonded/slipping zone ($z > \ell_d$)
σ_f^{res}	residual stress in the fibre in the bonded zone ($z > \ell_d$)
$\overline{\sigma}_m$	traction applied to the matrix at $z = 0$
σ_m^-	stress in the matrix in the debonded/slipping zone ($z < \ell_d$)
σ_m^+	stress in the matrix ahead of the debonded/slipping zone ($z > \ell_d$)
σ_m^{res}	residual stress in the matrix in the bonded zone ($z > \ell_d$)
τ_s	interfacial frictional sliding shear stress
$\tilde{\tau}_s$	apparent interfacial shear stress
ξ_F	frictional energy dissipation

Appendix A

In the following we wish to calculate the residual stresses at temperature T accounting for a pre-stress, σ_f^0 , applied to the fiber during the processing at temperature T_0. The pre-stress is applied to the fiber only, see Figure A-1. The matrix remains stress-free at temperature T_0. Thus, the resulting strain in the fiber and matrix after the application of the pre-stress to the fiber are thus given by Hooke's law

$$\varepsilon_f^0 = \frac{\sigma_f^0}{E_f} \qquad \text{and} \qquad \varepsilon_m^0 = 0\,. \qquad \text{(A-1)}$$

Following the application of the pre-stress the matrix is cured and the single fiber composite is cooled down to temperature T. The fiber is taken to possess a constant thermal expansion coefficient α_f. We assume that the matrix solidifies and obtains its full stiffness, given in terms of its Young's modulus E_m, during the curing. The matrix may undergo shrinkage before consolidation, but this will not be considered in the following, since residual stresses are not expected to build-up as long as the matrix is in a viscous state. The strain that the stress-free matrix material would undergo after solidification (usually contraction) is described in terms of a constant thermal expansion coefficient α_m.

As a part of the consolidation, the matrix is assumed to form a chemical bond to the fiber. Thus, the matrix cannot contract freely but must undergo the same strain change as the fiber. This constrain induces a resulting stress in the fiber, denoted σ_f^1 and a residual stress in the matrix, σ_m^1. Following consolidation and cool down to temperature T, the strain in the fiber ε_f^1 and the matrix ε_m^1 are given by

$$\varepsilon_f^1 = \alpha_f (T - T_0) + \frac{\sigma_f^1}{E_f} \qquad \text{and} \qquad \varepsilon_m^1 = \alpha_m (T - T_0) + \frac{\sigma_m^1}{E_m}\,. \qquad \text{(A-2)}$$

The strain changes are obtained from (A-1) and (A-2) as

$$\Delta\varepsilon_f^1 = \varepsilon_f^1 - \varepsilon_f^0 = \alpha_f (T - T_0) + \frac{\sigma_f^1}{E_f} - \frac{\sigma_f^0}{E_f} \quad \text{and} \quad \Delta\varepsilon_m^1 = \varepsilon_m^1 - \varepsilon_m^0 = \alpha_m (T - T_0) + \frac{\sigma_m^1}{E_m}\,. \quad \text{(A-3)}$$

Taking the thermal expansion coefficients as know material properties we can determine σ_f^1 and σ_m^1 by the two conditions: The strain changes after matrix consolidation have to be identical, $\Delta\varepsilon_f^1 = \Delta\varepsilon_m^1$, and the stresses σ_f^1 and σ_m^1 must be in force balance with the applied stress σ_f^0. This leads to

$$\sigma_f^1 = \sigma_f^0 - \frac{(1 - V_f) E_m}{E_c} E_f \Delta\varepsilon^T \qquad \text{and} \qquad \sigma_m^1 = \frac{V_f E_m}{E_c} E_f \Delta\varepsilon^T\,, \qquad \text{(A-4)}$$

where

$$\Delta\varepsilon^T = (\alpha_f - \alpha_m)(T - T_0)\,. \qquad \text{(A-5)}$$

is the mismatch strain.

Finally, the pre-stress is released. This is equivalent to adding a pressure (a negative stress) to the free fiber end. This creates a stress change to both the fiber and the matrix, denoted $\Delta\sigma_f^2$ and $\Delta\sigma_m^2$, respectively. Again the two conditions must be fulfilled: force balance and the fiber and matrix undergo the same strain change: $\Delta\varepsilon_f^2 = \Delta\varepsilon_m^2$, where the strain changes are given by Hooke's law

$$\Delta\varepsilon_f^2 = \frac{\Delta\sigma_f^2}{E_f} \qquad \text{and} \qquad \Delta\varepsilon_m^2 = \frac{\Delta\sigma_m^2}{E_m}. \tag{A-6}$$

Solving for $\Delta\sigma_f^2$ and $\Delta\sigma_m^2$ we find:

$$\Delta\sigma_f^2 = -\frac{V_f E_f}{E_c}\sigma_f^0, \qquad \text{and} \qquad \Delta\sigma_m^2 = -\frac{V_f E_m}{E_c}\sigma_f^0. \tag{A-7}$$

The final stress state, the residual stresses in the fiber and matrix, σ_f^{res} and σ_m^{res}, are obtained by adding the two stress fields (assuming linearity), Eq. (A-4) and (A-7):

$$\sigma_f^{res} = \sigma_f^1 + \Delta\sigma_f^2 \qquad \text{and} \qquad \sigma_m^{res} = \sigma_m^1 + \Delta\sigma_m^2. \tag{A-8}$$

The result is:

$$\sigma_f^{res} = \frac{(1-V_f)E_m}{E_c}\left\{\sigma_f^0 - E_f\Delta\varepsilon^T\right\} \qquad \text{and} \qquad \sigma_m^{res} = -\frac{V_f E_m}{E_c}\left\{\sigma_f^0 - E_f\Delta\varepsilon^T\right\}. \tag{A-9}$$

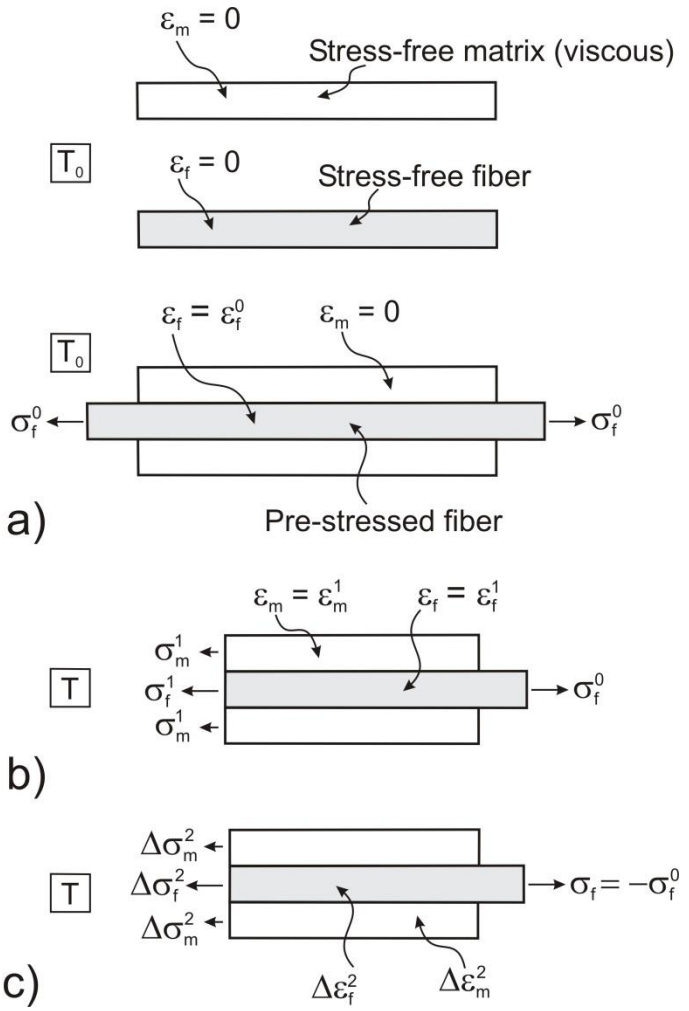

Figure A-1. Sketch of stress and strain during the processing of single fiber composite specimen with a pre-stressed fiber. (a) Pre-stress is applied at temperature T_0, (b) the stresses in balance at temperature T, (c) additional stresses induced as negative pre-stress is applied.

In the absence of pre-tension, (A-9) reduces to

$$\sigma_f^{res} = -\frac{(1-V_f)E_m}{E_c} E_f \Delta\varepsilon^T \qquad \text{and} \qquad \sigma_m^{res} = \frac{V_f E_m}{E_c} E_f \Delta\varepsilon^T . \qquad \text{(A-10)}$$

Obviously, (A-9) and (A-10) have very similar forms. It follows that experiments conducted with pre-tension ($\sigma_f^0 \neq 0$) can be analyzed as a problem without pre-tension by substituting

$$\Delta\tilde{\varepsilon}^T = -\frac{\sigma_f^0}{E_f} + \Delta\varepsilon^T , \qquad \text{(A-11)}$$

i.e., treating $\Delta\tilde{\varepsilon}^T$ as an "apparent" mismatch strain in the data analysis. When parameters e.g. ($\mathcal{G}_c^i$, τ_s and $\Delta\tilde{\varepsilon}^T$) are identified from experimental data, the true mismatch strain can be obtained from

$$\Delta\varepsilon^T = \Delta\tilde{\varepsilon}^T + \frac{\sigma_f^0}{E_f} . \qquad \text{(A-12)}$$

Finally, it follows from (A-9) that the residual stresses σ_f^{res} and σ_m^{res} vanish when the pre-stress are chosen as:

$$\sigma_f^0 = E_f \Delta\varepsilon^T . \qquad \text{(A-13)}$$

References

[1] Feih S, Wei J, Kingshott P and Sørensen BF 2005 *Composites part A* **36** 245
[2] Kim BW, Nairn JA 2002 *Journal of Composite Materials* **36** 1825
[3] Parthasarathy TA, Jero PD, and Kerans RD 1991 *Scripta Metall. Mater* **25** 2457
[4] Tripathi D, Jones F R 1998 *J. Mater. Sci*. **33** 1
[5] Kelly A and Tyson WR 1965 *Journal of the Mechanics and Physics of Solids* **13** 329
[6] Gao YC, Mai YW and Cotterell B 1988 *J. Appl. Mathematics and Physics (ZAMP)* **39** 550
[7] Hsueh CH 1990 *Materials Science and Engineering* **A123** 1
[8] Hutchinson JW and Jensen HM 1990 *Mechanics of Materials* **9** 139
[9] Graciani E, Mantic V, Paris F and Varna J 2009. *Comp. Sci. Techn.* **69** 2514
[10] Kessler H, Schüller T, Beckert W and Lauke B 1999 *Comp. Sci. Techn.* **59** 2231
[11] Nairn JA 2000 *Advanced Composite Letters* **9** 373
[12] Wu W, Verpoest I and Varna J 2000 *Comp. Sci. Techn.* **60** 351
[13] Budiansky B, Hutchinson JW and Evans AG 1986 *J. Mech. Phys. Solids* **34** 167
[14] Sørensen BF 2016, *Mechanics of Materials*, submitted for publication
[15] Prabhakaran DRT, Gupta M Lilholt H Sørensen BF and Mahajan P 2013 Experiments and analyses for determining fibre/matrix interface parameters in composites *34th Risø International Symposium on Materials Science, "Processing of fibre composites – challenges for maximum materials performance*. eds. B Madsen, H Lilholt, Y Kusano, S Fæster and B Ralph, Department of Wind Energy, Technical University of Denmark, Roskilde, Denmark, pp. 341-8
[16] Marshall D B, Shaw MC and Morris WL 1992 *Acta Metall. Mater.* **40** 443